China Ocean Eng., Vol. 25, No. 4, pp. 669 − 678

DOI 10.1007/s13344-011-0053-2, ISSN 0890-5487

Estimation of Turbulent Kinetic Energy Dissipation Rate in the Bottom Boundary Layer of the Pearl River Estuary*

LIU Huan (刘　欢)[a, b, 1], WU Chao-yu (吴超羽)[a] and REN Jie (任　杰)[a, c]

[a] *Research Center of Coastal Ocean Science and Technology*, *Sun Yat-sen University*, *GuangZhou 510275*, *China*

[b] *School of Environmental Science and Engineering*, *Sun Yat-sen University*, *Guangzhou 510275*, *China*

[c] *School of Marine Science*, *Sun Yat-sen University*, *GuangZhou 510275*, *China*

(Received 16 February 2011; received revised form 22 July 2011; accepted 26 September 2011)

ABSTRACT

A structure function approach is applied to estimate the turbulent kinetic energy (TKE) dissipation rate in the bottom boundary layer of the Pearl River Estuary (PRE). Simultaneous measurements with an acoustic Doppler velocimeter (ADV) supplied independent data for the verification of the structure function method. The results show that, 1) the structure function approach is reliable and successfully applied method to estimate the TKE dissipation rate. The observed dissipation rates range between 8.3×10^{-4} W/kg and 4.9×10^{-6} W/kg in YM01 and between 3.4×10^{-4} W/kg and 4.8×10^{-7} W/kg in YM03, respectively, while exhibiting a strong quarter-diurnal variation. 2) The balance between the shear production and viscous dissipation is better achieved in the straight river. This first-order balance is significantly broken in the estuary by non-shear production/dissipation due to wave-induced fluctuations.

Key words: *structure function*; *turbulent kinetic energy dissipation rate*; *bottom boundary layer*; *Pearl River Estuary*

1. Introduction

The tidal bottom boundary layer (BBL) flow is an important process in hydrodynamics, sediment transport, water quality and ecological issues in estuaries. The turbulent kinetic energy (TKE) dissipation rate, ε, is one of the key descriptive parameters of turbulence, and it is a controlling factor for the entire turbulent budget. Thus, understanding and modeling of ocean flows, pollutant dispersal and biological processes rely on the knowledge of the turbulence characteristics near the bottom (Lozovatsky and Femando, 2002; Kang *et al*., 2002).

Although the tidal BBL structure and dynamics have been investigated extensively in coastal oceanography and engineering (Cacchione *et al*., 2006; Burchard *et al*., 2008), measuring of turbulence parameters in the estuary and ocean is far from being a standard method. Several means to measure the turbulence and flow characteristics near the BBL have been developed, some involving direct measurements, others relying on an assumed velocity profile or turbulence characteristics. Generally speaking, the methods to estimate TKE dissipation rate can be generalized into four types: inertial dissipation method, microstructure profiler method, variance method and structure function method. Assuming a balance between turbulent kinetic energy production and dissipation, one can estimate the

* This study was financially supported by the National Natural Science Foundation of China (Grant No. 41006050), the China Postdoctoral Science Foundation (Grant No. 20090460799) and the Fundamental Research Funds for the Central Universities (Grant No. 11lgpy59).

1 Corresponding author. Email: liuhuan_80@hotmail.com

dissipation rate in the inertial range of the vertical velocity spectrum which is measured by acoustic Doppler velocimeter (ADV) (Doron *et al*., 2001, Nimmo *et al*., 2005). This method relies on the existence of sufficient separation between the dissipation range and energy-containing scale, and the shortcoming of this method is that the vertical shear cannot be estimated from a single instrument. Vertical profiles of turbulence parameters are obtained by shear and temperature microstructure profilers, such as FLY profiler (Simpson *et al*., 1996), SWAMP (Peters, 2003), and MSS (Kocsis *et al*., 1999). This method requires repeated profiling in order to obtain stable averages of statistical quantities. Moreover, it is restricted to the measurement of shallow water (< 10 m) because the water depth should be sufficient to keep microstructure profiler fall freely. To overcome these disadvantages new measuring technologies were developed. Acoustic Doppler Current Profiler (ADCP) is the most popular, and has been used very extensively (Lu and Lueck, 1998; Stacey *et al*., 1999). The use of four-beam instruments measures three velocity components and estimates turbulent parameters via the variance method. This approach assumes the horizontal homogeneity of the horizontal velocity and the second order moments of the turbulent velocities. However, estimates of Reynolds stresses and TKE production rate are susceptible to contamination by tilt of the instrument in anisotropic turbulence (Williams and Simpson, 2004; Nidzieko *et al*., 2005). The structure function was initially developed for estimation of the dissipation rate in atmospheric studies (Sauvageot, 1992). Wiles *et al*. (2006) applied this method to ADCP measurements in a shelf sea with strong tidal forcing. But the high Doppler noise of the ADCP restricts the application to environments with high turbulence. The PC-ADP is an extremely high precision profiler that has been designed primarily for boundary layer studies. It uses the pulse-to-pulse coherent processing method thus can produce high precision velocity data with small cells (1.6 cm) and rapid sampling (1 Hz). In recent years, Mohrholz *et al*. (2008) applied the structure function approach to the estimate of the TKE dissipation rate from PC-ADP beam velocities.

In order to study the dynamics in BBL, the TKE dissipation rate and its temporary and spatial variations in the Pearl River Estuary (PRE), we deployed several observations on a bottom-mounted tripod at the Huangmaohai Estuary in July, 2007. In this contribution, we present the estimates of the TKE dissipation rates from PC-ADP and ADV measurements in the BBL.

2. Structure Function Method

In a homogeneous turbulent flow the velocity difference between two points separated by a distance r is mainly determined by turbulent eddies of a spatial scale near r. A second order structure function $D(z,r)$ can be defined at a location z by using the turbulent velocity u',

$$D(z,r)=\overline{\left[u'(z)-u'(z+r)\right]^2}\,. \tag{1}$$

Assuming that the velocity difference is large due to eddies with a length scale comparable to r and an associated velocity scale of u'_r,

$$D(z,r)\sim(u'_r)^2\,. \tag{2}$$

The Taylor cascade theory relates the characteristic length scale and characteristic velocity scale of isotropic turbulent eddies in the inertial sub range with the dissipation rate ε (Taylor, 1937;

Gargett, 1999),

$$\varepsilon \sim (u'_r)^3 / r \ . \tag{3}$$

Combining Eq. (1) with Eq. (3) one can derive a relationship between the structure function $D(z,r)$ and the TKE dissipation rate ε,

$$D(z,r) = \mathrm{C}\varepsilon^{2/3} r^{2/3}, \tag{4}$$

where C is a constant, which in atmospheric and oceanic studies has been found to be between 2.0 and 2.2 (Sauvageot, 1992; Saddoughi and Veeravalli, 1994). In this paper $\mathrm{C} = 2.1$ is used. It should be mentioned that Eq. (4) is only valid for the inertial subrange, i.e. $\eta \ll r \le l_0$ where η is the scale of dissipation (Kolmogorov microscale) and l_0 is the vertical scale of the largest energy containing eddies (integral scale).

The structure function approach was applied to each of the three PC-ADP beams. For each depth bin z_i, the structure function $D(z,r)$ is calculated by using a centered difference scheme,

$$D(z_i, r_k) = \overline{\left[u'(z_{i-k}) - u'(z_{i+k})\right]^2} \tag{5}$$

where i is the depth cell, k is the interval cell, and $r_k = 2 \cdot k \cdot$ bin size.

According to Eq. (4), the sets of $D(z,r)$ were fitted to an equation of the form,

$$D(z,r) = ar^{2/3} + n \ , \tag{6}$$

with

$$a = \mathrm{C}\varepsilon^{2/3} \ , \tag{7}$$

As shown in Fig. 1, in order to find a value for *a*. *n* is an offset which represents an uncertainty largely due to inherent Doppler noise and other errors in the PC-ADP velocity estimates (or due to non-turbulent velocity fluctuations, e.g. waves) (Wiles *et al*., 2006).

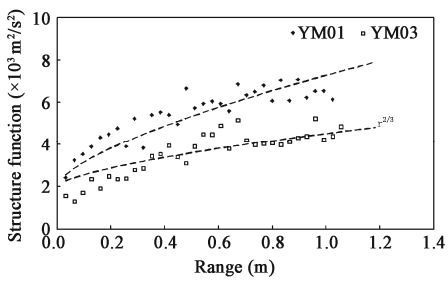

Fig. 1. $r^{2/3}$ fit on along beam PC-ADP data.

The raw beam velocities are temporally averaged over the averaging interval and then this mean is subtracted from the raw beam velocities. Afterwards, the TKE dissipation rates are calculated for each single beam of the PC-ADP, and then spatially average over the three beams within each depth cell.

3. Region Setting and Field Observation

The Huangmaohai Estuary, located in the western part of the PRE, is connected through a rock-bound outlet of 'Yamen' to the Yingzhouhu channel, further upstream to the Tanjiang River (Fig.

2a). The Tanjiang River is 248 km long, with a mean bed slope of 0.45 ‰. The long and narrow channel of Yingzhouhu is 25 km long, 1.5~2.1 km wide and 8~15 m deep. The Huangmaohai Estuary narrows exponentially from the bay mouth with a width of approximately 20 km to the head at the 'Yamen' with a width of only 0.6 km (Liu *et al.*, 2009). The fresh water discharging into the Yingzhouhu channel comes predominantly from the Tanjiang River, with an annual mean runoff of 19.6 billion m^3 into the Huangmaohai Estuary. A semidiurnal astronomical tide M_2 predominates in the estuary.

Data were collected for 25 h at each of the four sites (YM01~04) with period of July 17~22, 2007 (Fig. 2a). Since the PC-ADP parameters setting, only the results at site YM01 (17~18, July) and YM03 (20~21, July) will be discussed in this study. Site YM01 is located at the upper estuarine section and YM03 on the lee side (in the ebb direction) of an alluvial island in the upper Yingzhouhu channel. The mean water depth during the surveys is 4.7 m and 6.9 m at two sites YM01 and YM03, respectively. The tidal range is approximately 1.8 m at the Yanan gauging station. Wind vectors during the surveys indicate that the mean wind speed and directional range are respectively 6.0 ± 1.6 m/s and 170~230° at site YM01, and 2.7 ± 5.1 m/s and 180~270° at site YM03. The southern and southwestern winds predominated, roughly in the direction of the flood current. Whitecap sometimes occurred on the sea surface. Shipboard CTD profiling shows that the vertically homogeneous, well-mixed water column predominated during the surveys. Vertically stratified structures occurred primarily near the slack tides at the site YM01. Salinity contrasts are less than 0.2‰ at site YM03, so salinity stratification may be excluded from the processes acting on turbulence properties in the river. The surveys of two CTD sets fastened to the tripod indicate that the near-bed layer can be roughly viewed as a well-mixed layer.

A bottom-mounted instrumental tripod (Fig. 2b) was used to observe the BBL flows (mean and turbulence flows), turbidity, temperature and salinity. A Sontek/YSI PC-ADP with a central frequency of 1.5 MHz was down-looking fixed on the frame at the level of 1.3 m above the bottom to measure the near-bed mean velocities. The averaging interval and profile interval were both set to be 1s, burst interval of 900 s, 600 (YM01) and 300 (YM03) profiles per burst, cell size of 1.6 cm, and blanking distance of 5 cm. Two Nortek ADV were fastened to two legs of the tripod to observe the 3D turbulence velocity components at the level of 0.15 m above bed. We selected the ADV performance characteristics as the sampling rate is 64 Hz; sampling period is 300 s; burst interval is 900 s. In the present study, only data of one ADV were used to verify the results derived from PC-ADP.

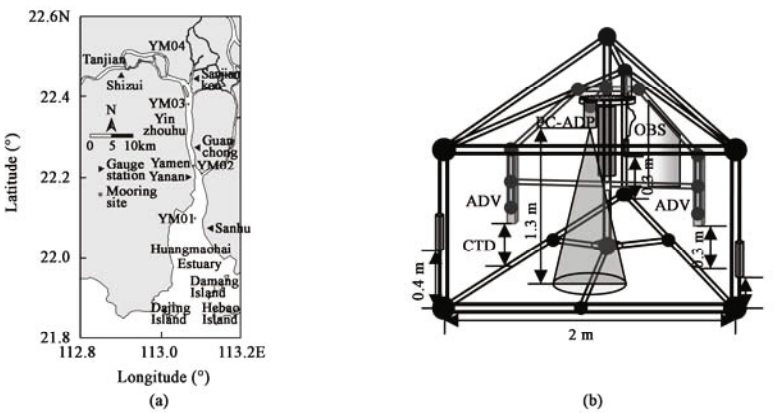

Fig. 2. Sketch map for the site of the survey station and work platform.

4. Results and Discussions

4.1 Averaging Time

For the calculation of the TKE dissipation rates by using structure functions, the velocity differences have to be averaged over a period. It must be long enough to give statistical reliability but short enough that the time series can be assumed stationary. With the observed mean velocity of about 0.6 m/s an eddy of 0.3 m size (Liu *et al*., 2008) needs about 5 s to pass a beam of PC-ADP.

In order to estimate the lower limit of suitable averaging times, dissipation rates were calculated for increasing averaging times from 5 to 300 s. For this test two ebb maximum periods were selected (17 Jul. 2007 18:30 to 18:40, YM01; 20 Jul. 2007 13:00 to 13:05, YM03). For a depth cell at the level of 0.15 m (the same level of the ADV) above the bottom the dissipation rates were estimated for increasing averaging times from 5 s to 300 s (Fig. 3). The dissipation rate was underestimated when averaging times less than 50 s, since it was influenced by a part of the low-frequency velocity fluctuations. With increasing averaging times the dissipation rate tends to its 300 s mean value. Mohrholz *et al*. (2008) indicated that the difference is about zero of 600 s mean value for averaging times longer than 100 s. The averaging time is set to 300 s in this study.

4.2 Range r

The impact of range r on the dissipation rate was estimated also from the same time periods as mentioned above. The minimum of range r is twice the bin size of 0.032 m in our case, and the maximum range of r is 1.184 m restricted by the height of PC-ADP. For a depth cell in the center of the PC-ADP profiling range the dissipation rates were estimated for increasing rang from 0.032 m up to 1.184 m. It is indicated that the dissipation rate decreases rapidly with the increasing of range r for $r < 0.2$ m, and the difference is one order of magnitude. The dissipation rate stabilized gradually in the r range between 0.2 m and 1 m, then showed an upward tendency for $r > 1$ m (Fig. 4). It was expected that in case of unstratified conditions and isotropic turbulence the estimates of the dissipation rate do not depend on the used range if $\eta \ll r \le l_0$. To use data as much as possible and keep stability on the dissipation rate estimates, the range of structure functions was restricted to 0.2 m.

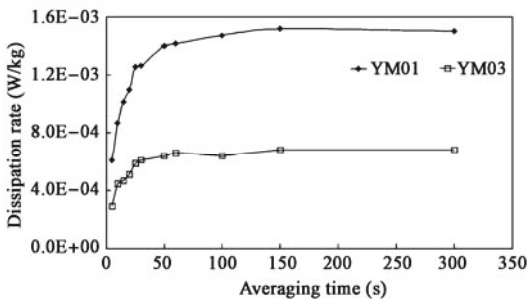

Fig. 3. Variation of the dissipation rates with varying averaging intervals.

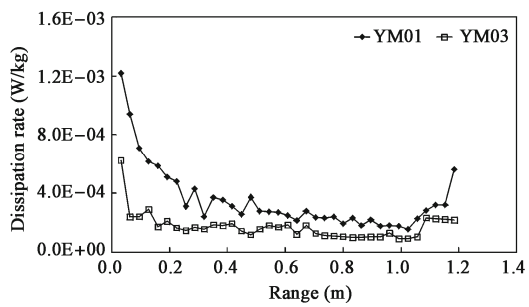

Fig. 4. Variation of the dissipation rates with varying range.

4.3 Comparison of Dissipation Rates

The feasibility and reliability of the structure function approach to estimate the TKE dissipation rates were tested by a comparison between dissipation rates derived from PC-ADP and ADV. The data were compared with each other at the measuring depth of 0.15 m above the bottom. The dissipation rates derived from ADV may be estimated in terms of the turbulence energy cascade in the inertial subrange, called the inertial dissipation technique (Nimmo *et al*., 2005),

$$\varepsilon = \frac{2\pi}{U}\alpha^{-3/2}\overline{f^{5/2}S^{3/2}(f)}, \tag{8}$$

where U is the mean velocity, f is the frequency, α is the one-dimensional Kolmogorov universal constant and $\alpha \approx 0.71$, and $S(f)$ is the energy spectral density at the frequency f.

Fig. 5 shows that 1) the dissipation rates from PC-ADP compared well with those from the ADV, and the correlation coefficient is 0.65 (YM01) and 0.67 (YM03), respectively. 2) Generally the PC-ADP estimates were about 5 times larger than the ADV results. This is probably due to the frequency of PC-ADP is lower than that of ADV, and it measured the larger eddy. On the other hand, the ambiguity errors in the velocity measured by PC-ADP may be increased by increasing the sampling rate and decreasing the bin size (Lacy and Sherwood, 2004). 3) The linear relationship between the dissipation rate from PC-ADP and from ADV at site YM03 is better than that of site YM01. Shipboard CTD profiling shows that, the vertically homogeneous, well-mixed water column predominated during the surveys at YM03, but vertically stratified structures occurred primarily near the slack tides at the site YM01 (Liu *et al*., 2009). This suggests that the estimation of the dissipation rate by the structure function may return incorrect results for stratified water. Furthermore, using the structure function method in the BBL may contain uncertainties because the size of the energy-containing eddies is limited by the distance from the boundary.

4.4 TKE Dissipation Rate in the Bottom Boundary Layer

We used the averaging time $t = 300$ s and a small range $r = 0.2$ m for calculations of ε. Fig. 6 shows the temporal and spatial variation of the dissipation rates and the northward components of the mean velocity measured by the ADV. It can be seen that 1) The dissipation rates were higher in the bottom layer and lower in the upper layer. In general, strong shear induced eddies near the bed and propagated upward throughout the entire water column. Therefore the turbulent characteristics such as turbulent intensity, Reynolds stress and the TKE dissipation rate decline from the bottom to the upper water. 2) The dissipation rates almost exactly follow the near bottom velocity magnitude. For the PRE where the semi-diurnal tidal current is dominant, the dissipation rates exhibit a strong quarter-diurnal variation. The variations of the mean vertical dissipation rates during 25 h are significant, 8.3×10^{-4}~4.9×10^{-6} W/kg at site YM01 and 3.4×10^{-4}~4.8×10^{-7} W/kg at site YM03, respectively. 3) The mean magnitude of the dissipation rate is larger at the estuarine site YM01, and is smaller at the riverine site YM03. Furthermore the time variations of the velocity show that tidal asymmetry is more evident at site YM01. This suggests that ambient flows, e.g. estuarine gravity circulation, wind-driven circulation, and wave may enhance the dissipation rate.

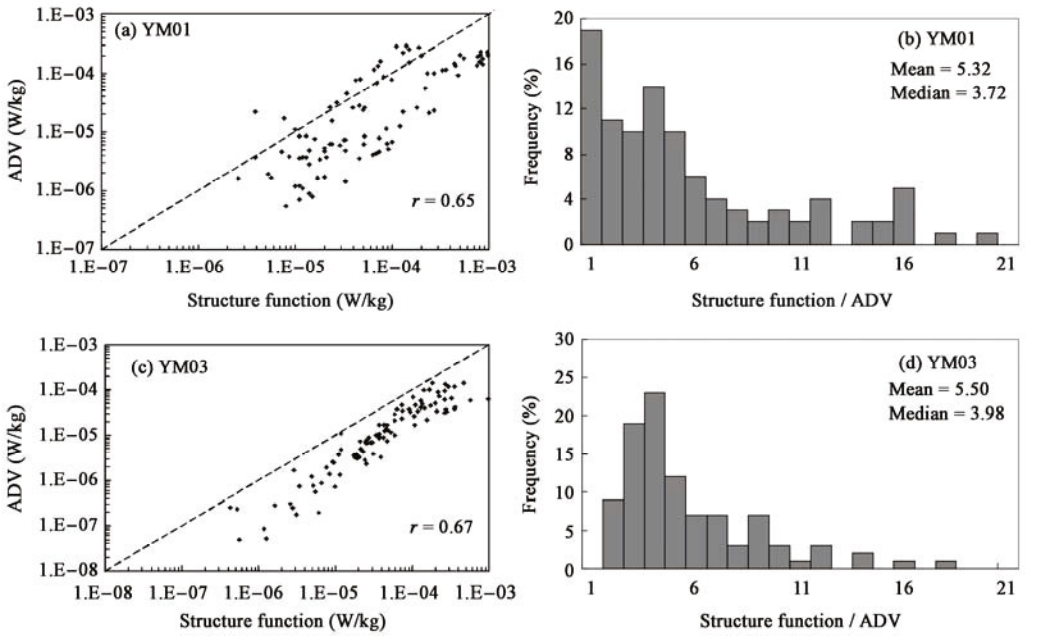

Fig. 5. Comparison between dissipation rates derived from structure function and ADV.

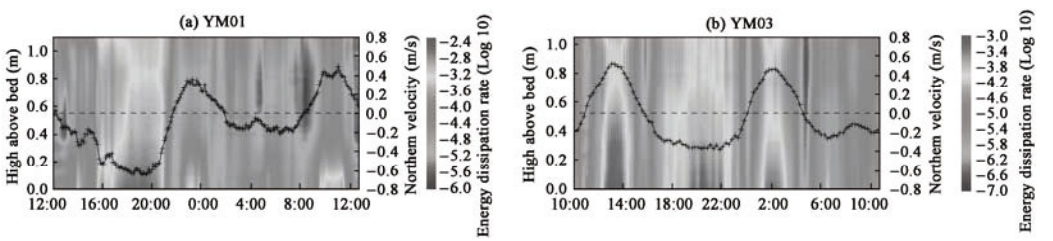

Fig. 6. Variation of the dissipation rate for the bottom boundary layer in a tidal cycle.

4.5 Energy Balance

In the fully-mixed turbulent BBL, the TKE shear production is assumed to be approximately equal to the viscous dissipation (Tennekes and Lumely, 1972; Trowbridge *et al*., 1999). But in the concentrated benthic layer, the buoyancy dissipation to the suspended load may be an important contributor to the TKE balance, giving

$$P = D + B\,, \tag{9}$$

where the shear production $P = -\overline{u_{\mathrm{e}}' w'}\frac{\partial}{\partial z}\overline{u}_{\mathrm{e}} - \overline{u_{\mathrm{n}}' w'}\frac{\partial}{\partial z}\overline{u}_{\mathrm{n}}$, the viscous dissipation $D = -\rho_0 \varepsilon$, and the buoyancy flux $B = -g\overline{\rho' w'}$. ρ' is the density fluctuation, w' is the fluctuation of the vertical velocity, subscripts e and n are the eastward and northward velocity, respectively.

Fig. 7 depicts the correlation of dissipation rates and shear productions estimate from PC-ADP for the site YM01 and YM03. The upper layer is 1.13 m above the bed and the bottom layer is 0.15m above the bed. It can be seen that 1) The dissipation rates and the shear productions have a pretty good

correlation, and the correlation coefficient r is higher than 0.5. This indicates that, the dissipation rates derived from structure function are consistent with the shear productions. 2) In the estuary (YM01), the viscous dissipation is larger than shear production, and in this case there exists other energy production, e.g. the rate of working of pressure fluctuations induced by waves. The coherences between the pressure fluctuation and the vertical turbulence velocity also show that the vertical turbulence component at the estuarine site YM01 was apparently disturbed by waves within the low-frequency (Liu *et al*., 2009). The first-order balance is in a good agreement in the straight river (YM03). When buoyancy is negligible in the turbulent BBL, energy is transferred from the mean shear flow to turbulence by the action of processes of the Reynolds stress on the mean shear flow, and consequently in a steady state turbulent dissipation is directly related to shear stress.

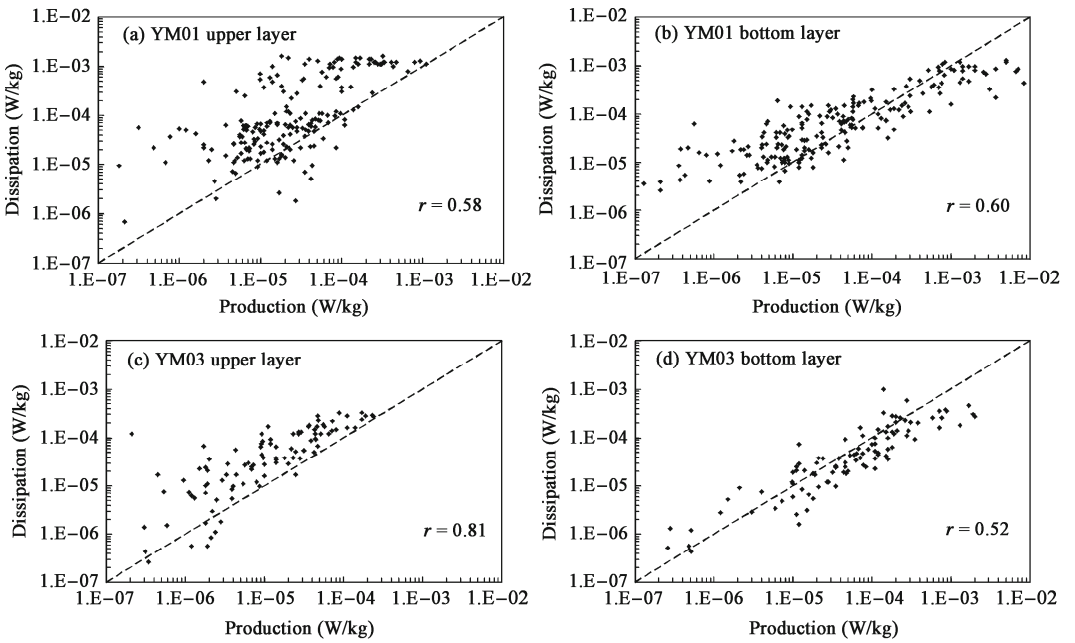

Fig. 7. Turbulent energy balance in the bottom boundary layer.

5. Conclusions

From the calculations and comparison of the TKE dissipations obtained by PC-ADP and ADV in the BBL of the PRE, we obtain the following conclusions:

1) The structure function method was successfully applied to PC-ADP data in order to estimate TKE dissipation rates, which is well fit with the results derived from ADV. The averaging time of 300 s and the range of 0.2 m are suitable to estimate the dissipation rate in the tidal BBL within 1 m above the bed.

2) The TKE dissipation rates have significant variations between 8.3×10^{-4} and 4.9×10^{-6} W/kg (YM01), and between 3.4×10^{-4} and 4.8×10^{-7} W/kg (YM03), respectively. For the PRE where the semi-diurnal tidal current is dominant, the dissipation rates exhibit a strong quarter diurnal variation.

3) The turbulent energy balance has significant difference in estuary and river. The viscous dissipation is larger than shear production in the estuary, suggesting that other non-shear energy sources (e.g. wave stirring) are supplied to the viscous dissipation. But in the straight river without density stratification, the balance between shear production and dissipation is in a good agreement.

References

Burchard, H., Craig, P. D., Gemmrich, J. R., van Haren, H., Mathieu, P-P., Meier, H. E. M., Nimmo Smith, W. A. M., Prandke, H., Rippeth, T. P., Skyllingstad, E. D., Smyth, W. D., Welsh, D. J. S. and Wijesekera, H. W., 2008. Observational and numerical modeling methods for quantifying coastal ocean turbulence and mixing, *Progress in Oceanography*, **76**(4): 399~442.

Cacchione, D. A., Sternberg, R. W. and Ogston, A. S., 2006. Bottom instrumented tripods: history, applications, and impacts, *Continental Shelf Research*, **26**(17-18): 2319~2334.

Doron, P. K., Bertuccioli, L., Katz, J. and Osborn, T. R., 2001. Turbulence characteristics and dissipation estimates in the coastal ocean bottom boundary layer from PIV data, *J. Phys. Oceanogr.*, **31**(8): 2108~2134.

Gargett, A. E., 1999. Velcro measurement of turbulence kinetic energy dissipation rate epsilon, *J. Atmos. Oceanic Technol.*, **16**(12): 1973~1993.

Kang, S. K., Foreman, M. G. G., Lie, H. J., Lee, J. -H., Cherniawsky, J. and Yum, K. -D., 2002. Two-layer tidal modeling of the Yellow and East China Seas with application to seasonal variability of the M2 tide, *J. Geophys. Res.*, **107**(C3): 3020~3037.

Kocsis, O., Prandke, H., Stips, A., Simon, A. and Wüest, A., 1999. Comparison of dissipation of turbulent kinetic energy determined from shear and temperature microstructure, *Journal of Marine Systems*, **21**(1-4): 67~84.

Lacy, J. R. and Sherwood, C. R., 2004. Accuracy of a Pulse-Coherent Acoustic Doppler Profiler in a wave-dominated flow, *Journal of Atmospheric and Oceanic Technology*, **21**(9): 1448~1461.

Liu, H., Wu, C. Y. and Xu, W. M., 2008. Research of turbulent flow integral length scale on the bottom boundary layer in the Pearl River, *The Ocean Eng.*, **26**(4): 125~131. (in Chinese)

Liu, H., Wu, C. Y., Xu, W. M. and Wu, J. X., 2009. Contrasts between estuarine and river systems in near-bed turbulent flows in the Zhujiang (Pearl River) Estuary, China, *Estuarine, Coastal and Shelf Science*, **83**(4): 591~601.

Lozovatsky, I. and Fermando, H. J. S., 2002. Turbulent mixing on a shallow shelf of the Black Sea, *J. Phys. Oceanogr.*, **32**(3): 945~956.

Lu, Y. and Lueck, R. G., 1998. Using a broadband ADCP in a tidal channel, Part II: turbulence, *Journal of Atmospheric and Oceanic Technology*, **16**, 1568~1579.

Mohrholz, V., Prandke, H. and Lass, H. U., 2008. Estimation of TKE dissipation rates in dense bottom plumes using a Pulse Coherent Acoustic Doppler Profiler (PC-ADP) — Structure function approach, *Journal of Marine Systems*, **70**, 217~239.

Nidzieko, N. J., Fong, D. A. and Hench, J. L., 2005. Comparison of Reynolds stress estimates derived from standard and fast-ping ADCPs, *Journal of Atmospheric and Oceanic Technology*, **23**(6): 854~861.

Nimmo Smith, W. A. M., Katz, J. and Osborn, T. R., 2005. On the structure of turbulence in the bottom boundary layer of the coastal ocean, *J. Phys. Oceanogr.*, **35**(1): 72~93.

Peters, H., 2003. Broadly distributed and locally enhanced turbulent mixing in a tidal estuary, *J. Phys. Oceanogr.*, **33**(9), 1967~1977.

Saddoughi, S. G. and Veeravalli, S. V., 1994. Local isotropy in turbulent boundary layers at high Reynolds number, *J. Fluid Mech.*, **268**, 333~372.

Sauvageot, H., 1992. Radar Meteorology, Artech House, Norwood(MA).

Simpson, J. H., Crawford, W. R., Rippeth, T. P., Campbell, A. R. and Cheok, J. V. S., 1996. The vertical structure of turbulent dissipation in shelf seas, *J. Phys. Oceanogr*., **26**(8): 1579~1590.

Stacey, M. T., Monismith, S. G. and Burau, J. R., 1999. Measurements of Reynolds stress profiles in unstratified tidal flow, *J. Geophys. Res*., **104**(c5): 10933~10949.

Taylor, G. I., 1937. The statistical theory of isotropic turbulence, *J. Aeronaut*., **4**, 311~315.

Tennekes, H. and Lumley, J. L., 1972. *A First course in Turbulence*, MIT Press, Cambridge, 300.

Trowbridge, J. H., Geyer, W. R., Bowen, M. M. and Willams A. J., 1999. Near-bottom turbulence measurements in a partially mixed estuary: Turbulent energy balance, velocity structure, and along-channel momentum balance, *J. Phys. Oceanogr*., **29**(12): 3056~3072.

Wiles, P. J., Rippeth, T. P., Simpson, J. H. and Hendricks, P. J., 2006. A novel technique for measuring the rate of turbulent dissipation in the marine environment, *Geophysical Research Letter*, **33**(2-1): 1~5.

Williams, E. and Simpson, J. H., 2004. Uncertainties in estimates of Reynolds stress and TKE production rate using the ADCP variance method, *Journal of Atmospheric and Oceanic Technology*, **21**(2): 347~357.